




## Article

# Structural Consequences of Post-Synthetic Modification of $\text{Cu}_2\text{P}_3\text{I}_2$

Gregory R. Schwenk <sup>†</sup>, John T. Walters <sup>†</sup> and Hai-Feng Ji <sup>\*</sup>

Department of Chemistry, Drexel University, Philadelphia, PA 19104, USA

<sup>\*</sup> Correspondence: [hj56@drexel.edu](mailto:hj56@drexel.edu); Tel.: +1-215-895-2562; Fax: +1-215-895-1265<sup>†</sup> These authors contributed equally to this work.

**Abstract:** In an attempt to widen the family of Phosphorus Metal Halides ( $\text{M}_x\text{P}_y\text{X}_z$ ) and enable new applications, post-synthetic modifications to the  $\text{M}_x\text{P}_y\text{X}_z$ ,  $\text{Cu}_2\text{P}_3\text{I}_2$  have been reported. While such a technique suggests access to an entirely new family of  $\text{M}_x\text{P}_y\text{X}_z$ -based materials, we report, in this work, that the ion-exchange process seemingly influences important properties such as the crystallographic pattern and vibrational modes.

**Keywords:** phosphorus; Phosphorus Metal Halide; ion-exchange;  $\text{Cu}_2\text{P}_3\text{I}_2$ ;  $\text{Ag}_2\text{P}_3\text{I}_2$ ; powder X-ray diffraction; Raman Spectroscopy

## 1. Introduction

Since the isolation and subsequent vast applications of phosphorene [1], research interest in low-dimensional phosphorus-based materials has increased dramatically. While initial studies focused heavily on phosphorene and its bulk analog, black phosphorus (BP), other allotropic forms have proven successful in various applications and have begun to garner interest. As evidenced by Differential Scanning Calorimetry (DSC) measurements, red phosphorus (RP) may exist in one of five proposed polymorphs denoted by roman numerals from I to V [2]. While types I–III lack full structural elucidation, type I has been characterized as an effective FET [3] and type II has displayed potential in photocatalysis [4]. Type III has only been reportedly observed once by DSC and has not been replicated in literature since [2]. Type IV and V are fully structurally resolved and have been employed in a wide range of applications, including cell imaging and optoelectronic devices [5–8].

One-dimensional nanorod structures of both type II and IV RP have been reported. However, exposing the nanorods to ambient conditions affords similar oxidation effects to those observed with black phosphorus, limiting their stability and application. Bearing similar rod-like structures to type II and IV RP, Phosphorus Metal Halides ( $\text{M}_x\text{P}_y\text{X}_z$ ) adduct structures with CuI maintain similar properties, but with enhanced stability [9,10]. Integral to these structures, a phosphorus nanorod is isolated inside a framework of CuI which may be solubilized in aqueous KCN solutions to afford the individual nanorods their own “allotrope” [11]. Owing to the nanorod isolation in the CuI framework, these materials have even been characterized as stable humidity sensors without suffering passivation effects [12]. Since many of these materials have been limited to a surrounding CuI framework, methods that promote different metal halides open a window of opportunity for various applications depending on the constituent metal.

In an attempt to widen the application of such materials by replacing  $\text{Cu}^+$  with other metal ions, post-synthetic modifications to the  $\text{M}_x\text{P}_y\text{X}_z$ ,  $\text{Cu}_2\text{P}_3\text{I}_2$  have reportedly facilitated a near 98% ion exchange with silver [13]. While such a technique suggests access to an entirely new family of  $\text{M}_x\text{P}_y\text{X}_z$ -based materials, the ion-exchange process seemingly influences important properties such as the crystallographic pattern and vibrational modes. Herein, we report the experimentally obtained Raman spectra for  $\text{Cu}_2\text{P}_3\text{I}_2$  and compare that with the reported post-synthetic  $\text{Ag}_2\text{P}_3\text{I}_2$ . Differences in the spectra of  $\text{Cu}_2\text{P}_3\text{I}_2$  and



**Citation:** Schwenk, G.R.; Walters, J.T.; Ji, H.-F. Structural Consequences of Post-Synthetic Modification of  $\text{Cu}_2\text{P}_3\text{I}_2$ . *Micro* **2023**, *3*, 256–263. <https://doi.org/10.3390/micro3010018>

Academic Editors: Nurettin Sahiner and Zlatan Denchev

Received: 29 November 2022

Revised: 1 February 2023

Accepted: 15 February 2023

Published: 1 March 2023



**Copyright:** © 2023 by the authors. Licensee MDPI, Basel, Switzerland. This article is an open access article distributed under the terms and conditions of the Creative Commons Attribution (CC BY) license (<https://creativecommons.org/licenses/by/4.0/>).

$\text{Ag}_2\text{P}_3\text{I}_2$  prompted further characterization through powder XRD, cyclic current voltage (CIV), and SEM imaging, which overwhelmingly pointed to the conclusion that the ion exchange of  $\text{Cu}_2\text{P}_3\text{I}_2$  is ineffective in producing pure isotopic  $\text{Ag}_2\text{P}_3\text{I}_2$ .

## 2. Experimental

### 2.1. $\text{Cu}_2\text{P}_3\text{I}_2$ Synthesis

The Chemical Vapor Transport (CVT) process was performed as previously reported by this lab [9]. In brief, samples were prepared using stoichiometric amounts of CuI and type I, amorphous, red phosphorus (a-RP). For smaller-diameter borosilicate ampoules, a yield of 100 mg was targeted (80.4 mg CuI and 19.6 mg a-RP), and for larger-diameter ampoules, a 250 mg yield was targeted (201.0 mg CuI and 49 mg a-RP). Both scales of reaction yielded similar results. These reagents were added to a borosilicate tube, which was subsequently backfilled with Argon then sealed under vacuum as an ampoule. These ampoules were spaced evenly in the center of a muffle furnace placed orthogonally to the heating element (Figure 1A). The ends of the ampoule were pointed to the heating elements so that they were closer to the heating elements than the center, creating a heating gradient over the length of the ampoule to allow chemical vapor transport. The furnace was heated rapidly to 373 K then heated to 723 K at a rate of 5 K/min. The furnace was then heated at a rate of 1 K/min until it reached 823 K, followed by a rate of 0.5 K/min until it reached 853 K. This temperature was then held for 48 hr. The furnace was then cooled at a rate of 0.33 K/min until it reached 773 K, where it was held for 18 hr (heating/cooling curve shown in Figure 1B). The furnace was then cooled at a rate of 5 K/min until it reached 473 K, at which point the furnace was turned off and the sample was left to equilibrate with room temperature.

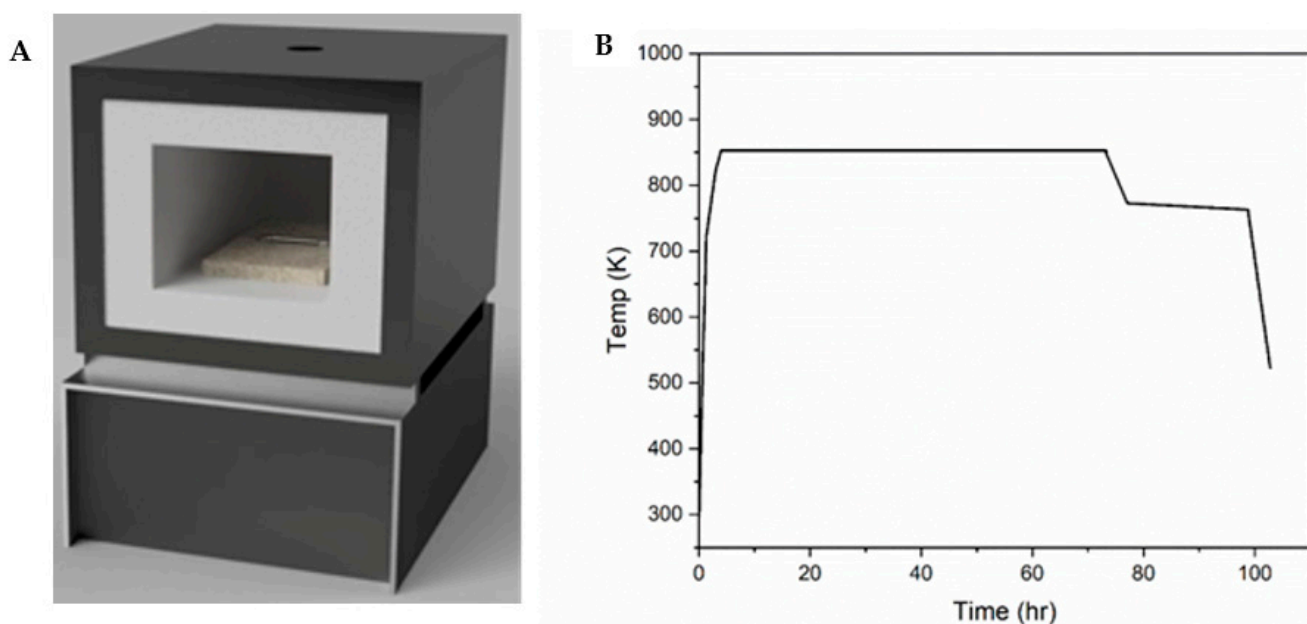


**Figure 1.** Reaction ampoules were oriented orthogonally to the heating elements in the walls of the muffle furnace (A) and the typical heating/cooling curve associated with  $\text{Cu}_2\text{P}_3\text{I}_2$  (B).

### 2.2. Post-Synthetic Modification

As reported by Möller and Jeitschko [10], the copper cations in  $\text{Cu}_2\text{P}_3\text{I}_2$  nanowires could be displaced with silver cations by adding the wires to a 10% (*w/w*) aqueous solution of  $\text{AgNO}_3$  with excess KCN by reaction (1).



After a few hours, the solution was centrifuged, and the supernatant liquid was removed. The wires were subsequently washed in methanol after which the suspension was centrifuged, and the supernatant was removed. This allows for formation of post-synthetic  $\text{Ag}_2\text{P}_3\text{I}_2$  by modifying the previously synthesized  $\text{Cu}_2\text{P}_3\text{I}_2$ .

### 2.3. Electrical Characterization

Single-wire devices were prepared on a Si/SiO<sub>2</sub> (n-doped) wafer containing 2 gold electrodes separated by a 10  $\mu\text{m}$  channel. When fixed to the electrode surfaces with a graphene-based conductive glue, the single wire spanned the channel; any current resulting from the potential difference between the two electrodes is required to pass through the single wire to reach the ground. Instrument probes were connected to copper wires that were glued to the gold plates with the graphene-based conductive glue. Current *v.* Potential plots (IV) were generated using a Keithley 2636A Dual-channel System SourceMeter Instrument (Keithley Instruments, Inc. Cleveland, OH, USA). Source and drain probes were attached to the copper wires of the devices and current was measured against a time-varying electric potential. Cyclic IV (CIV) plots were generated using a VersaSTAT 3 Potentiostat Galvanostat (Princeton Applied Research, Oak Ridge, TN, USA). Similar to how the IV plots were generated, source and drain probes were attached to the copper wires of the devices and current was measured against a time-varying electric potential such that the final potential matched the initial. A total of five cycles were run per trial.

### 2.4. Raman Spectroscopy

Several analytical methods have been employed to characterize the various phosphorous allotropes, the most common being X-Ray Diffraction (XRD), both powder and single crystal, and Raman Spectroscopy [14–20]. While XRD patterns provide structural insight, the unique variety of these phosphorus allotropes lead to distinct Raman-active vibrational modes that allow for further differentiation. Using computational data, many have attempted to interpret these spectra to provide specific vibrational modes for each Raman band [14].

Samples of  $\text{Cu}_2\text{P}_3\text{I}_2$  and  $\text{Ag}_2\text{P}_3\text{I}_2$  were loaded onto a glass microscope slide. A Renishaw RM-2000 Vis Raman Spectrometer (Gloucestershire, UK) was used to probe the observed Raman shifts in each sample. Optimal conditions were observed in the absence of ambient light and when samples were exposed to 10% laser strength of a 633 nm beam. Resulting shifts were collected through an 1800 mm diffraction grating. Spectral acquisitions occurred with 10+ accumulations comprised of 10-second exposure times.

### 2.5. Powder X-ray Diffraction (P-XRD)

Samples of  $\text{Cu}_2\text{P}_3\text{I}_2$  and  $\text{Ag}_2\text{P}_3\text{I}_2$  were prepared via CVT and post-synthetic modification respectively, as described in the Experimental section. Approximately 100 mg of each sample were ground into fine powders with the use of a mortar and pestle. Powders were placed on glass sample holders and prepared for P-XRD analysis. P-XRD was performed with a Rigaku MiniFlex (Tokyo, Japan) equipped with a Cu K $\alpha$  radiation source. Diffraction patterns were acquired in the range of 3–50° with a step increase of 0.02° and a dwell time of 1 s. Predicted XRD patterns were generated in Mercury 2022.1.0 (Build 343014; CDC, Boston, MA, USA).

## 3. Discussion

The Raman spectrum collected for  $\text{Cu}_2\text{P}_3\text{I}_2$  (Figure 2A) shows unique vibrational modes that are separate and distinguishable from other phosphorus-based materials. Presently, to the authors' knowledge, there are no literature sources in which the Raman profile of  $\text{Cu}_2\text{P}_3\text{I}_2$  is reported, and therefore, these bands are unassigned. However, the observed Raman activity is consistent with the window in which various P allotropes show activity [16,17]. Conversely, the  $\text{Ag}_2\text{P}_3\text{I}_2$  spectrum (Figure 2B) is highly unresolved and contains only a broad peak in the same window in which individual  $\text{Cu}_2\text{P}_3\text{I}_2$  bands

occur. This stark difference suggests that while the  $\text{Cu}_2\text{P}_3\text{I}_2$  is a more highly regular repeating structure, the  $\text{Ag}_2\text{P}_3\text{I}_2$  generated through post-synthetic modification has regions of higher variability. Because this procedure produces a material that is highly irregular, this method is likely ineffective in generating an isotypic silver analog for  $\text{Cu}_2\text{P}_3\text{I}_2$  as originally suggested [10]. The high degree of irregularities is suspected to originate from the fracturing of wires as a result of the larger  $\text{Ag}_2\text{P}_3\text{I}_2$  unit cell and potential solubilizing of the CuI shell when exposed to the KCN solution, both of which will be discussed in greater detail below [10,11,13]. Additional studies may be required to fully determine the Raman modes so that the deformation mechanisms may be validated.

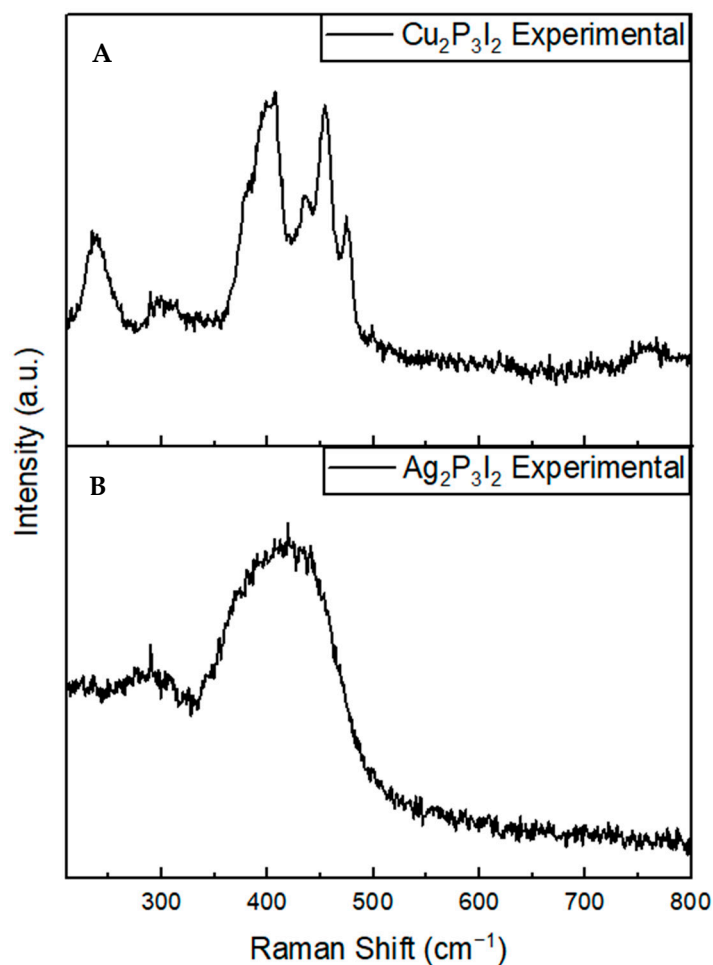


**Figure 2.** The Raman spectrum of a sample of  $\text{Cu}_2\text{P}_3\text{I}_2$  produced by chemical vapor transport (A) and  $\text{Ag}_2\text{P}_3\text{I}_2$  produced by post-synthetic modification (B).

The P-XRD patterns of  $\text{Cu}_2\text{P}_3\text{I}_2$  and  $\text{Ag}_2\text{P}_3\text{I}_2$  (Figure 3C) corroborates what has been suggested by the difference in the Raman profiles—long range periodicity is not maintained after post-synthetic modifications have been made. The experimental pattern for  $\text{Cu}_2\text{P}_3\text{I}_2$  was acquired from a sample prepared via chemical vapor transport as described in the experimental section. The simulated pattern was generated in the crystallographic software Mercury 2022.1.0 (Build 343014), from a CIF previously acquired by our lab [9]. The experimental sample was then converted to  $\text{Ag}_2\text{P}_3\text{I}_2$  by the post-synthetic procedure outlined in the experimental section. Notably, the  $\text{Ag}_2\text{P}_3\text{I}_2$  pattern reveals a few bands that do not match with the  $\text{Cu}_2\text{P}_3\text{I}_2$  pattern, as well as a broad amorphous region. Most importantly, the characteristic peaks of  $\text{Cu}_2\text{P}_3\text{I}_2$  are completely gone, proving long range order is significantly reduced. For further investigation, the  $\text{Cu}_2\text{P}_3\text{I}_2$  CIF file was modified in Mercury 2022.1.0 (Build 343014) to replace the  $\text{Cu}^+$  ions with  $\text{Ag}^+$  ions while maintaining

isotypic structure (as suggested in the literature), and a resulting simulated pattern for  $\text{Ag}_2\text{P}_3\text{I}_2$  was generated for comparison (Figure 3C, top).

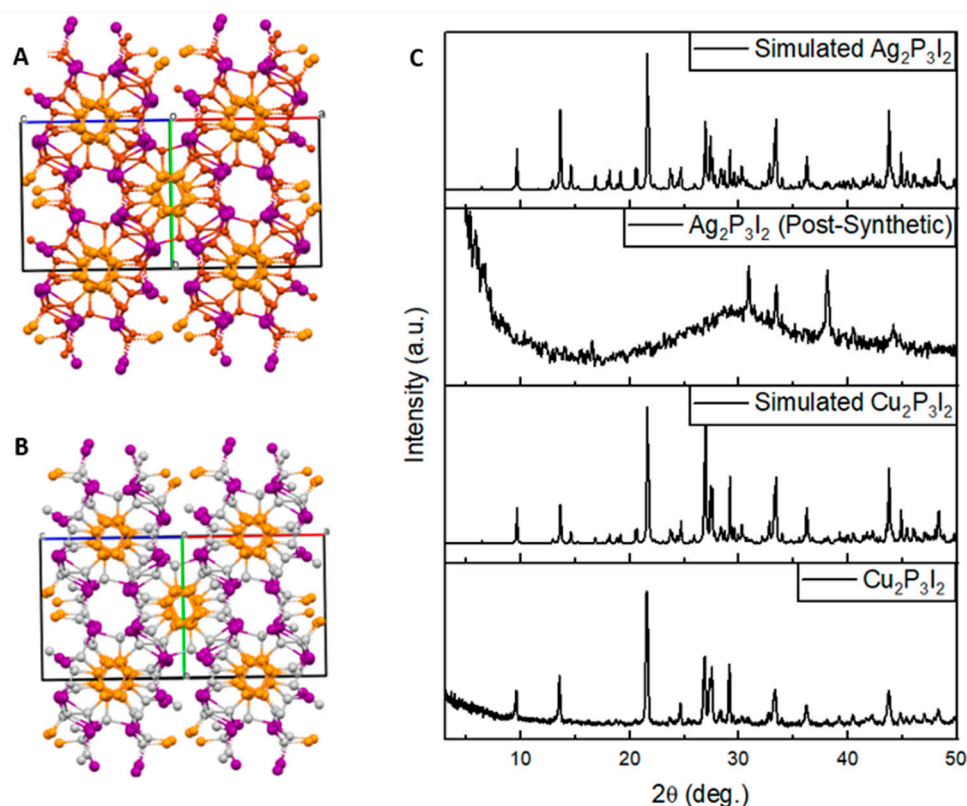


**Figure 3.** Crystal structures of  $\text{Cu}_2\text{P}_3\text{I}_2$  (A) and the modified isotypic  $\text{Ag}_2\text{P}_3\text{I}_2$  (B) as well as their corresponding PXRD predicted and experimental patterns (C).

As briefly mentioned previously, one major issue with this synthesis is the potential solubilizing of the  $\text{CuI}$  framework by the use of  $\text{KCN}$ . This reagent is necessary, however, for the formation of the complex  $[\text{Ag}(\text{CN})_2]^-$  which mitigates the amount of surface impurities (compared to just  $\text{AgNO}_3$  without  $\text{KCN}$ ). Since the pilot study of these  $\text{M}_x\text{P}_y\text{X}_z$  materials, it has been observed that the  $\text{CuI}$  framework can be removed by stirring the solid in a solution of  $\text{KCN}$ , affording a reddish-brown precipitate composed of P nanorods [11]. As a result, it is reasonable to suspect that the  $\text{CuI}$  framework is prone to degradation during the ion exchange process which occurs in a  $\text{KCN}$  solution. To corroborate this,  $\text{Cu}_2\text{P}_3\text{I}_2$  was added to a silver nitrate solution followed by the addition of  $\text{KCN}$ . The solution immediately developed a reddish-brown color, which is not present if the reagents are added in the correct order. This color change supports prior suggestions that a side reaction between the  $\text{KCN}$  and the  $\text{Cu}_2\text{P}_3\text{I}_2$  is occurring and is observed in the extraction of the P nanorod from  $\text{Cu}_2\text{P}_3\text{I}_2$ .

The other reason for the poor resolution of the Raman is the fracturing of the material. It was found that the post-synthetically modified material was exceptionally brittle and fragile when compared to the precursor ( $\text{Cu}_2\text{P}_3\text{I}_2$ ); the wires fractured readily under minimal force such as being picked up with forceps. A major contributor to this fragility is likely the deformation seen from intercalating a larger cation into the structure. The unit cell volume of  $\text{Cu}_2\text{P}_3\text{I}_2$  is too small to accommodate the much larger silver cation without structural deformation. Möller and Jeitschko [10] reported that the cell volume increases from  $2711 \text{ \AA}^3$  to  $2998 \text{ \AA}^3$  as a result of the ion exchange, causing a deformation which weakens the material overall. The SEM images of the post-synthetically modified material presented in the Möller paper illustrate that the wires are not one continuous structure; rather, they are fractured into bundles of smaller fibers. As such, not only is the



KCN solution suspected to solubilize the metal halide outer layer, but, even after successful ion exchange, the inability to account for the new cell volume forces fracturing.

The post-synthetic modification approach has two further drawbacks separate from the structural issues: it is wasteful, and excess silver is plated onto the wire. To perform post-synthetic modification, a 10% (*w/w*) solution of silver nitrate must be generated, which comprises a great excess of silver. Much of this solution is wasted, and a new solution must be generated for each synthesis because silver nitrate solutions are UV-active and the silver cations reduce to elemental silver. Furthermore,  $\text{Cu}_2\text{P}_3\text{I}_2$  must first be generated, and all the copper from this pre-cursor becomes waste. A chemical vapor transport reaction would eliminate the need for an expensive reaction solution and the copper intermediate, generating a purer product with less waste. Admittedly, however, such CVT attempts were discussed and found fruitless [10].

As mentioned above, the post-synthetic modification of  $\text{Cu}_2\text{P}_3\text{I}_2$  necessitates the use of  $[\text{Ag}(\text{CN})_2]^-$  to avoid contamination of the surface with impurities (e.g.,  $\text{CuI}$ ,  $\text{AgI}$ ,  $\text{Ag}$ , etc.). However, by selecting the use of the silver complex, further structural deformations are incurred by the KCN solution and the cell volume of the exchanged product. As evidenced by XRD and Raman, long-range periodicity is sacrificed. In order to assess the implications of such deformations, the electrochemical profile of the material was assessed with a CIV scan from  $-2\text{ V}$  to  $+2\text{ V}$  (Figure 4).

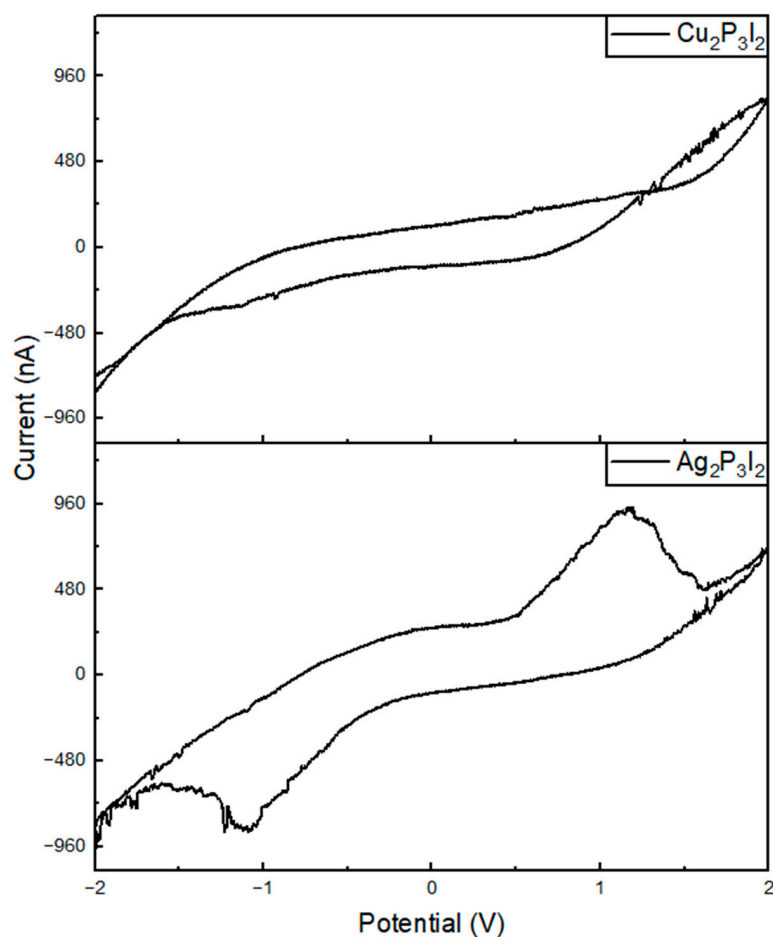


**Figure 4.** Cyclic IV curves for  $\text{Cu}_2\text{P}_3\text{I}_2$  produced by chemical vapor transport (**top**), and  $\text{Ag}_2\text{P}_3\text{I}_2$  produced by post-synthetic modification of  $\text{Cu}_2\text{P}_3\text{I}_2$  (**bottom**).

In the case of  $\text{Ag}_2\text{P}_3\text{I}_2$ , what appears to be redox activity can be observed. The activity is confined to the  $\text{Ag}_2\text{P}_3\text{I}_2$  material and moves depending on the applied voltage (Figures S1 and S2). Furthermore, the appearance of this shifting peak is not wholly consistent; it seems to appear for some batches of  $\text{Ag}_2\text{P}_3\text{I}_2$  but not for others. However, in

any case, the peak never occurs for  $\text{Cu}_2\text{P}_3\text{I}_2$ . Since there are a significantly large number of variables at play (i.e., surface impurities, KCN etching of the CuI layer, splintering, etc.) it is difficult to assign an explanation. Further studies will be conducted in which the CIV curve will be generated while simultaneously probing other properties of the material such as its Raman profile to identify the formation of any intermediate species that may play a role in the observed redox. Regardless, this observation corroborates the claim that structural deformations are induced by the post-synthetic modification process and illustrates implications this has on potential applications. These results highlight the need to develop  $\text{Ag}_2\text{P}_3\text{I}_2$ , and potentially other  $\text{M}_x\text{P}_y\text{X}_z$  structures, via chemical vapor transport if the materials' target application requires a high degree of crystallinity. It is worth noting, however, that the post-synthetic route may still be valid for applications that do not suffer from a lack of long-range crystallinity (i.e., potential antimicrobial activity of post-synthetically modified  $\text{Ag}_2\text{P}_3\text{I}_2$ ).

#### 4. Conclusions

The post-synthetic modification of  $\text{Cu}_2\text{P}_3\text{I}_2$  presents a potential to expand phosphorus metal halide structures to encompass metal halides besides CuI. While this is a noble effort, the present approach does not seem feasible in producing phase-pure  $\text{Ag}_2\text{P}_3\text{I}_2$  while maintaining isotypic character of its parent material. Herein, we have employed comparative XRD analysis to highlight the reduction in long-range periodicity after post-synthetic modification of  $\text{Cu}_2\text{P}_3\text{I}_2$  to  $\text{Ag}_2\text{P}_3\text{I}_2$  was performed. Additionally, we have corroborated these results with the apparent reduction of defined bands in the Raman profile of the material. This apparent structural deformation has been shown to limit the potential application of these materials by generating inconsistent phenomena in the CIV profile. Therefore, the results of this study highlight the need for synthetic routes that expand the phosphorus metal halide family without compromising its features. However, the post-synthetic route may still successfully provide access to a wider range of phosphorus metal halide materials so long as their target applications do not require crystallinity, such as catalysis.

**Supplementary Materials:** Supporting Information can be downloaded at: <https://www.mdpi.com/article/10.3390/micro3010018/s1>; Figure S1: Linear IV curves of  $\text{Ag}_2\text{P}_3\text{I}_2$  single-wire device; Figure S2: Redox peak shifting during CIV at various voltages; Figure S3: SEM images of post-synthetically modified  $\text{Ag}_2\text{P}_3\text{I}_2$ .

**Author Contributions:** G.R.S. and J.T.W. performed the experiments and analyzed the data. H.-F.J. provided the laboratory space and materials with which the experiments were conducted. All the authors have contributed to the design of the experiments, writing, and editing of the paper. All authors have read and agreed to the published version of the manuscript.

**Funding:** This research received no external funding.

**Institutional Review Board Statement:** Not Applicable.

**Informed Consent Statement:** Not Applicable.

**Data Availability Statement:** Not Applicable.

**Conflicts of Interest:** The authors declare no conflict of interest.

#### References

1. Liu, H.; Neal, A.T.; Zhu, Z.; Luo, Z.; Xu, X.; Tománek, D.; Ye, P.D. Phosphorene: An Unexplored 2D Semiconductor with a High Hole Mobility. *ACS Nano* **2014**, *8*, 4033–4041. [[CrossRef](#)] [[PubMed](#)]
2. Roth, W.L.; DeWitt, T.W.; Smith, A.J. Polymorphism of Red Phosphorus. *J. Am. Chem. Soc.* **1947**, *69*, 2881–2885. [[CrossRef](#)] [[PubMed](#)]
3. Amaral, P.E.M.; Nieman, G.P.; Schwenk, G.R.; Jing, H.; Zhang, R.; Cerkez, E.B.; Strongin, D.; Ji, H. High Electron Mobility of Amorphous Red Phosphorus Thin Films. *Angew. Chem. Int. Ed.* **2019**, *58*, 6766–6771. [[CrossRef](#)] [[PubMed](#)]
4. Zhaojian, S.; Zhang, B.; Yan, Q. Solution Phase Synthesis of the Less-Known Form II Crystalline Red Phosphorus. *Inorg. Chem. Front.* **2022**, *9*, 4385–4393. [[CrossRef](#)]

5. Smith, J.B.; Hagaman, D.; DiGuseppi, D.; Schweitzer-Stenner, R.; Ji, H. Ultra-Long Crystalline Red Phosphorus Nanowires from Amorphous Red Phosphorus Thin Films. *Angew. Chem. Int. Ed.* **2016**, *55*, 11829–11833. [[CrossRef](#)] [[PubMed](#)]
6. Amaral, P.E.M.; Hall, D.C.; Pai, R.; Król, J.E.; Kalra, V.; Ehrlich, G.D.; Ji, H.-F. Fibrous Phosphorus Quantum Dots for Cell Imaging. *ACS Appl. Nano Mater.* **2020**, *3*, 752–759. [[CrossRef](#)]
7. Schusteritsch, G.; Uhrin, M.; Pickard, C.J. Single-Layered Hittorf's Phosphorus: A Wide-Bandgap High Mobility 2D Material. *Nano Lett.* **2016**, *16*, 2975–2980. [[CrossRef](#)] [[PubMed](#)]
8. Lu, Y.-L.; Dong, S.; He, H.; Li, J.; Wang, X.; Zhao, H.; Wu, P. Enhanced Photocatalytic Activity of Single-Layered Hittorf's Violet Phosphorene by Isoelectronic Doping and Mechanical Strain: A First-Principles Research. *Comput. Mater. Sci.* **2019**, *163*, 209–217. [[CrossRef](#)]
9. Amaral, P.E.M.; Ji, H.-F. Stable Copper Phosphorus Iodide ( $\text{Cu}_2\text{P}_3\text{I}_2$ ) Nano/Microwire Photodetectors. *ChemNanoMat* **2018**, *4*, 1083–1087. [[CrossRef](#)]
10. Möller, M.H.; Jeitschko, W. Preparation, Properties, and Crystal Structure of the Solid Electrolytes  $\text{Cu}_2\text{P}_3\text{I}_2$  and  $\text{Ag}_2\text{P}_3\text{I}_2$ . *J. Solid State Chem.* **1986**, *65*, 178–189. [[CrossRef](#)]
11. Pfitzner, A.; Bräu, M.F.; Zweck, J.; Brunklaus, G.; Eckert, H. Phosphorus Nanorods—Two Allotropic Modifications of a Long-Known Element. *Angew. Chem. Int. Ed.* **2004**, *43*, 4228–4231. [[CrossRef](#)] [[PubMed](#)]
12. Schwenk, G.R.; Walters, J.T.; Ji, H.-F. Stable  $\text{Cu}_2\text{P}_3\text{I}_2$  and  $\text{Ag}_2\text{P}_3\text{I}_2$  Single-Wire and Thin Film Devices for Humidity Sensing. *Micro* **2022**, *2*, 183–190. [[CrossRef](#)]
13. Freudenthaler, E. Copper(I) Halide-Phosphorus Adducts: A New Family of Copper(I) Ion Conductors. *Solid State Ion.* **1997**, *101*, 1053–1059. [[CrossRef](#)]
14. Fasol, G.; Cardona, M.; Hönl, W.; von Schnering, H.G. Lattice Dynamics of Hittorf's Phosphorus and Identification of Structural Groups and Defects in Amorphous Red Phosphorus. *Solid State Commun.* **1984**, *52*, 307–310. [[CrossRef](#)]
15. Winchester, R.A.L.; Whitby, M.; Shaffer, M.S.P. Synthesis of Pure Phosphorus Nanostructures. *Angew. Chem.* **2009**, *121*, 3670–3675. [[CrossRef](#)]
16. Akahama, Y.; Kobayashi, M.; Kawamura, H. Raman Study of Black Phosphorus up to 13 GPa. *Solid State Commun.* **1997**, *104*, 311–315. [[CrossRef](#)]
17. Kornath, A.; Kaufmann, A.; Torheyden, M. Raman Spectroscopic Studies on Matrix-Isolated Phosphorus Molecules  $\text{P}_4$  and  $\text{P}_2$ . *J. Chem. Phys.* **2002**, *116*, 3323–3326. [[CrossRef](#)]
18. Ruan, B.; Wang, J.; Shi, D.; Xu, Y.; Chou, S.; Liu, H.; Wang, J. A Phosphorus/N-Doped Carbon Nanofiber Composite as an Anode Material for Sodium-Ion Batteries. *J. Mater. Chem. A* **2015**, *3*, 19011–19017. [[CrossRef](#)]
19. Shen, Z.; Hu, Z.; Wang, W.; Lee, S.-F.; Chan, D.K.L.; Li, Y.; Gu, T.; Yu, J.C. Crystalline Phosphorus Fibers: Controllable Synthesis and Visible-Light-Driven Photocatalytic Activity. *Nanoscale* **2014**, *6*, 14163–14167. [[CrossRef](#)] [[PubMed](#)]
20. Nilges, T.; Kersting, M.; Pfeifer, T. A Fast Low-Pressure Transport Route to Large Black Phosphorus Single Crystals. *J. Solid State Chem.* **2008**, *181*, 1707–1711. [[CrossRef](#)]

**Disclaimer/Publisher's Note:** The statements, opinions and data contained in all publications are solely those of the individual author(s) and contributor(s) and not of MDPI and/or the editor(s). MDPI and/or the editor(s) disclaim responsibility for any injury to people or property resulting from any ideas, methods, instructions or products referred to in the content.